ANALYSIS OF THE MICROSTRUCTURE AND DEFORMATION OF WOVEN COMPOSITES USING MICROFOCUS X-RAY DIFFRACTION

Robert J Young*, Sheng-Yuan Lei*, Prasad Potluri*, Stephen J Eichhorn*, James A Bennett*, Richard J Davies**

*School of Materials
University of Manchester
Manchester, M1 7HS, UK
**ESRF, Grenoble, France
robert.young@manchester.ac.uk

ABSTRACT

This paper presents an experimental approach, based on the techniques of Raman Spectroscopy and microfocus X-ray diffraction, for validating the micro-strains predicted by meso-scale FE models of textile composites. With the aid of these non-contact methods, local strains of individual reinforcing fibres can be determined. It is also shown how synchrotron microfocus X-ray diffraction can be employed to analyze fibre tilt and orientation within woven composites. It is found that local fibre strains are a function of off-axis angle and tow thickness. It is demonstrated that finite element analysis can be employed model accurately the dependence of fibre deformation upon fibre weave geometry in both plain and satin weave structures.

1. INTRODUCTION

There has been a recent surge in the use of composites in the aerospace industry stimulated by the Boeing 787 program, utilizing over 50% by weight of composites, and also with the recent Airbus 350 program. Unidirectional (UD) prepreg based laminates, consolidated in an autoclave, have been the principal material choice for the composites industry especially for aerospace applications – laminate analysis of UD composites is relatively straightforward with well established failure criteria and the design allowables. However, there are concerns about the damage tolerance and compression after impact (CAI) performance of UD composites, in addition to the high manufacturing and material costs. In recent years, composites industry has been pursuing a cost reduction strategy through various affordable composites initiatives, and at the same time trying to improve damage tolerance.

Textiles preforms, in the form of interlaced or stitched tow assemblies, are prime candidates for replacing UD prepregs in order to reduce costs and improve damage tolerance. A number of textile technologies including weaving, stitch bonding, braiding and 3D preforming have been evaluated in the 1990s through NASA's Advanced Composite Technology Program [1]. Textile preforms can be used in both prepreg and dry forms. In the dry form, textiles are easy to handle, have unlimited shelf life and easy to drape over complex surfaces. However, interlaced textiles in the form of woven or braided structures have complex tow geometry leading to complex strain fields around interlacements. Additional complexity arises from the fact that tows deform readily during draping/forming and consolidation processes leading to further changes in local strain fields. As a result, design methodology of textile composites is an order of magnitude more complex in comparison to well-established laminate analysis for unidirectional composites. This acts as an impediment to the widespread exploitation of textile composites, in spite of their techno-economic benefits.

Textile preforms that are commonly used for structural composites may be classified as interlaced and stitch-bonded. A third class of inter-looped preforms (weft/warp knitting) is seldom used for structural applications due to the presence of high crimp. Weaving produces a variety of orthogonally interlaced preforms, from plain to satin weaves, whereas braiding produces non-orthogonally interlaced preforms. In addition to these bidirectional broadcloth materials, 3D weaving and 3D braiding techniques are being used to produce multi-layer multi-directional preforms. Alternately, a set of orthogonal or multi-axial tows may be stitched together with a polyester thread using a stitch-bonding processes in order to produce the so-called Non Crimp Fabrics (NCF) (Figure 1).

Overall, interlaced preforms are superior to stitch-bonded in terms of their ability to drape uniformly in +/- directions and the resulting composites have superior damage tolerance and inter-laminar shear strength. However, the characteristic crimp (tow waviness) present in an interlaced structure leads to a reduction in in-plane modulus and strength in addition to resulting in complex stress concentrations. Stitched NCF composites, on the other hand, are expected to have superior in-plane modulus due to very low crimp. However, crimp angles of around 8^o have been reported for NCF composites as a result of ply nesting [2].

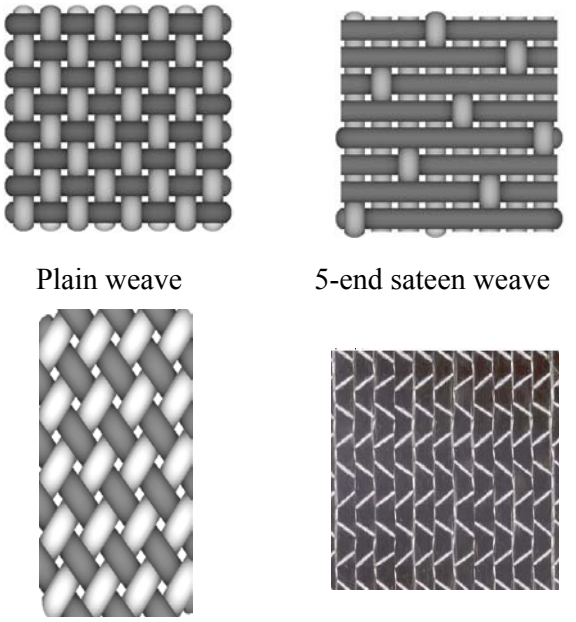

Figure 1: Common textile structures

2. MESO-SCALE MODELLING

The mechanical behaviour of heterogeneous materials can be simulated by homogenization methodologies by treating them as periodic structures and considering representative unit-cells with periodic boundary conditions. For example, fibre reinforced composites can be treated at two scales, micro-scale at fibre-matrix interface and at a macro-scale, with the micro- to macro-scale ratio (e) being very small. Asymptotic homogenization of the periodic structures involves micro-scale description of the boundary value problem and obtaining partial differential equations for macro-

scale displacement field as '*e*' approaches zero [3]. Both the spectral methods [4] and finite element methods [5] are used for solving the equations derived by the homogenization process, however, finite element methods are popular.

It can be shown mathematically that for periodic structures, the stress field and the deformation field can be decomposed into smooth macroscopic components and perturbed components.

$$\sigma(X) = S + \sigma^*(X)$$
$$F(X) = \Phi + F^*(X) \qquad (1)$$

where, $\sigma(X)$ is the local Piola-Kirchoff stress tensor and $F(X)$ is the local deformation gradient. $\sigma^*(X)$ and $F^*(X)$ are the oscillatory contributions. The homogenized tensors S and Φ are defined as the volume average of σ and F over the un-deformed unit cell. The main challenges in modelling textile composites are to create a unit cell with accurate tow geometry and fibre volume fractions and to predict the perturbed or oscillatory components of stress and deformation gradients.

For textile composites, the characteristic tow undulations are captured at the meso-scale. A representative volume element may be decomposed into individual sub-elements, containing warp tow segments, weft tow segments and resin pockets (Figure 2). Tow sub-elements are treated as transversely isotropic UD laminate while the resin pockets are treated as homogeneous.

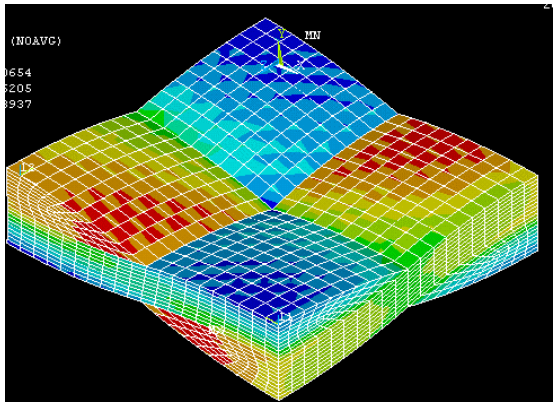

Figure 2: Unit-cell (resin pockets not shown)

3. EXPERIMENTAL

3.1 Raman Spectroscopy

Raman spectra were obtained from the woven composites, using a Renishaw Raman system 1000 with a 25 mW HeNe laser focused to around a 2 μm spot on the surface of the woven composites as described elsewhere [6]. The Raman band at 1610 cm^{-1} was used to map the fibre strains in the woven composites at different applied strains. The strain-induced Raman band shift rate of -4.6±0.5 cm^{-1}/% was used to convert the Raman wavenumber into fibre strain. Strain mapping was undertaken along the centre of one repeat unit in the woven aramid/epoxy composites as shown in Figure 3. The local strain distributions were measured at a variety of levels of overall strain.

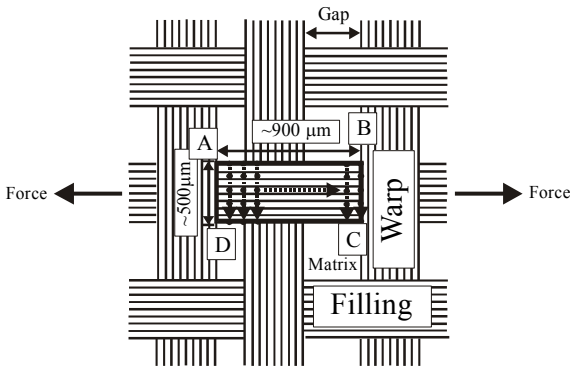

Figure 3: Illustration of one-dimensional strain mapping in a plain weave fabric lamina.

3.2 Synchrotron Microfocus X-ray Diffraction

The X-ray micro-diffraction experiments on the woven composites were conducted at the ESRF, Grenoble, France on beam-line ID13 as described elsewhere [7]. The beamline was configured with a monochromatic beam (0.1 nm wavelength), focused using compound refractive lenses. These provide a spot size at the focal position of 5 µm. The specimen was deformed in situ using a miniature materials tensile testing rig installed on the beamline's sample stage. Analysis of the diffraction data was performed using the FIT2D software application. Radial profiles were first generated which allowed the positions of the fibre meridional reflections to be determined. This enabled the subsequent calculation of lattice spacings in the fibre axis direction and hence the fibre crystal strain. Diffraction patterns were collected in a two-dimensional scan centred around the position of the drilled hole. This extended 8 mm along each axis with a step size of 200 µm. All data was collected using a MARCCD 165 area detector. Typical exposure times were approximately 1 s, normalized using an ionization chamber positioned upstream of the sample.

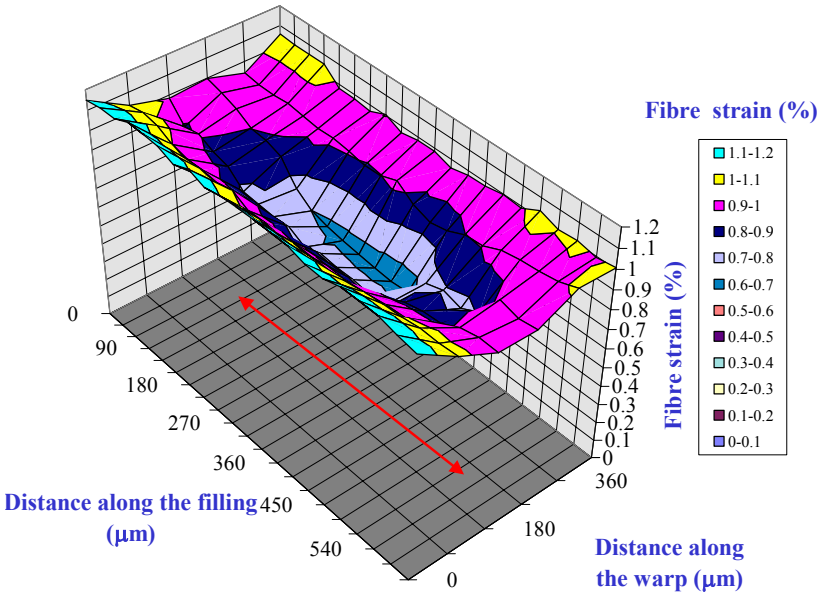

Figure 4: Distribution of fibre strain in a cell of the plain weave aramid composite at 1% overall strain.

4 RESULTS AND DISCUSSION

4.1 Raman Spectroscopy

Detailed mapping of the fibre strain distributions was undertaken as shown in Figure 4 for the defined cell from Figure 3 for a plain weave specimen loaded to 1% overall strain. It can be seen that the fibre strain is a maximum at the edges of the cell and falls to a minimum in the middle.

4.2 Modelling of the plain weave

A lenticular geometry (Figure 5) has been used in modelling the textile unit cell. The tow cross-section is described by two circular arcs, and the crossing tow is assumed to be in full contact. The gap between the adjacent tows has been assumed to be zero – this has been found to be a reasonable assumption as each tow spreads laterally to the available space during resin impregnation (unless a very loose fabric construction is used).

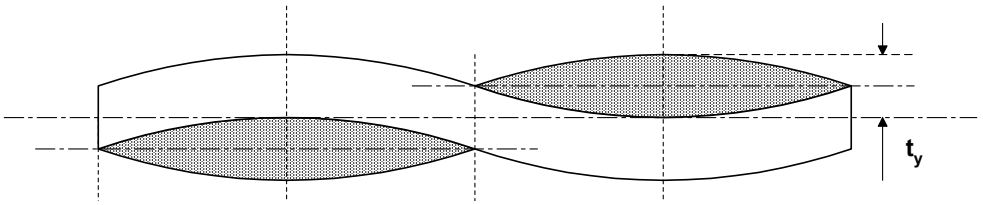

Figure 5. Lenticular geometry used for unit cell modeling in a plain-weave structure

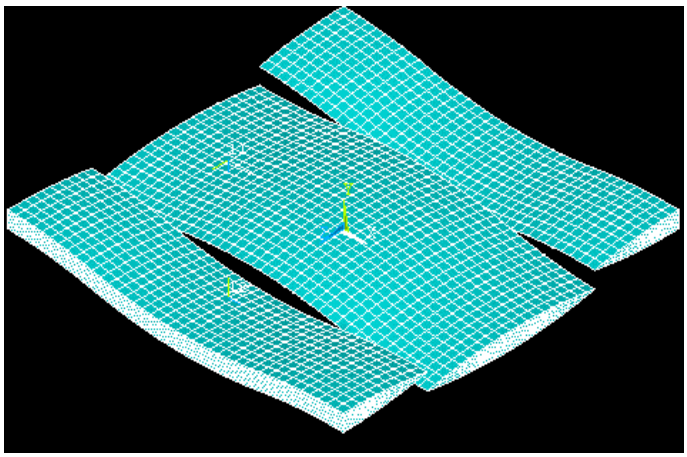

Figure 6: The weft tow (part of the unit cell)

The strains along the centreline of a woven composite at different strain levels were computed for the weft tows shown in Figure 6. The results are plotted in Figure 7 for different levels of overall strain. It can be seen that the form of the behaviour found experimentally in Figure 4 is followed but that the difference in strain at the edges of the cell compared with the centre of the tow are predicted to be larger than the measured values. This is currently the subject of more detailed analysis to obtain the full strain field verification.

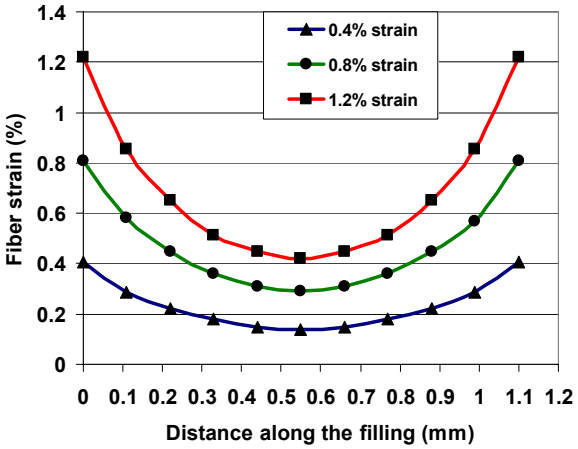

Figure 7: Computed strains along the tow centreline at different global strain values

4.3 X-ray Diffraction Analysis

Figure 8 shows an X-ray diffraction pattern obtained for a woven aramid composite consisting of two intersecting diffraction patterns corresponding to tows of fibres in orthogonal directions [8]. The following parameters can be determined from analysis of the diffraction patterns both before and after deformation:

- The local angle between the warp and weft fibres.
- The degree of fibre orientation in the warp and weft fibres.
- The out-of-plane tilt angle of the warp and weft fibres .
- The fibre strain in the warp and weft fibres.

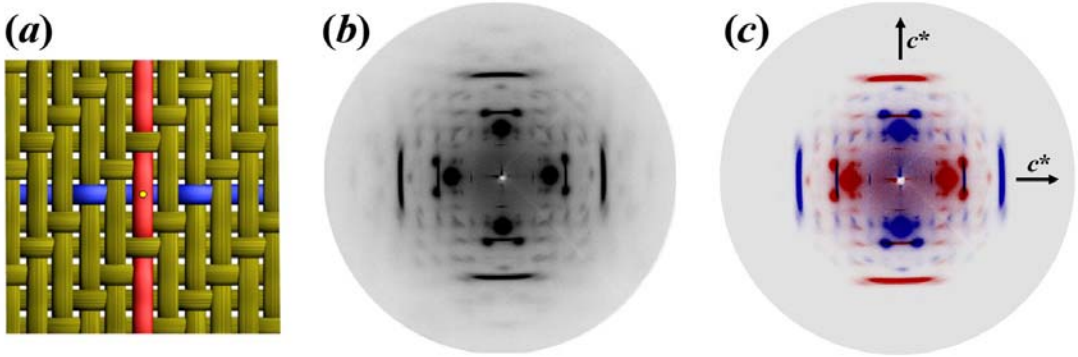

Figure 8: (a) Example of data collection from a position on the sample (indicated by a yellow circle) at which longitudinal (red) and transverse (blue) yarns are superimposed. The resulting diffraction pattern (b) shows a superposition of scattering contributions which can be separated by their angular offset (c). This allows the two yarn orientations, with their respective fibre axes denoted *c**, to be analysed independently

Figure 9 shows schematic scans across a woven aramid composite. Each individual diffraction pattern in the figure contains a range of information about the embedded PPTA fibres. By plotting different analysis parameters according to their real-space collection position on the sample, their spatial variation can be correlated with the sample's local geometry and stress fields. For example, preferred crystalline domain orientation within the fibres allows macroscopic yarn orientations to be determined.

Furthermore, provided there is a sufficiently high angular difference, the superposition of different yarn orientations within the detector plane can be resolved separately. This allows information to be obtained from warp and weft yarns independently when studying woven composite geometries.

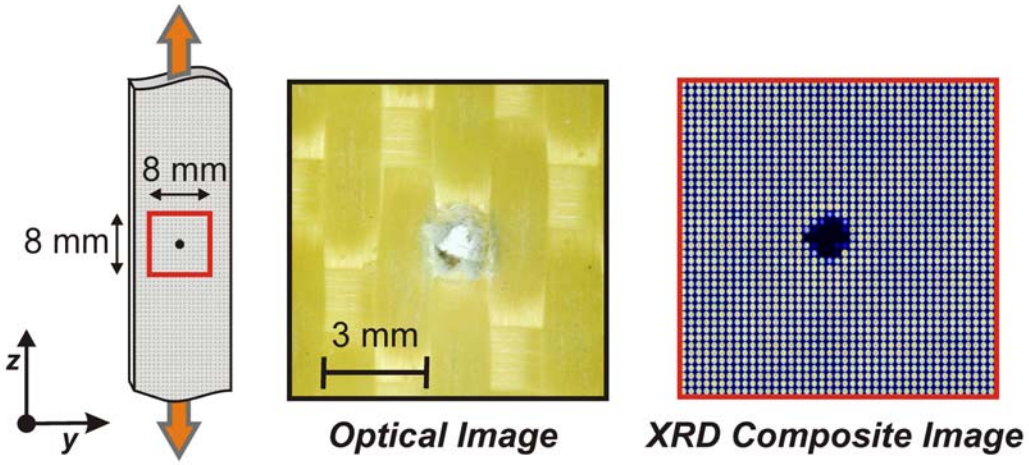

Figure 9: Schematic of the data collection region with respect to the position of the drilled hole and composite deformation geometry. An optical micrograph of a similar 8×8 mm^2 region of a satin weave composite lamina is also shown along with a composite image comprising individual diffraction patterns placed according to data collection position.

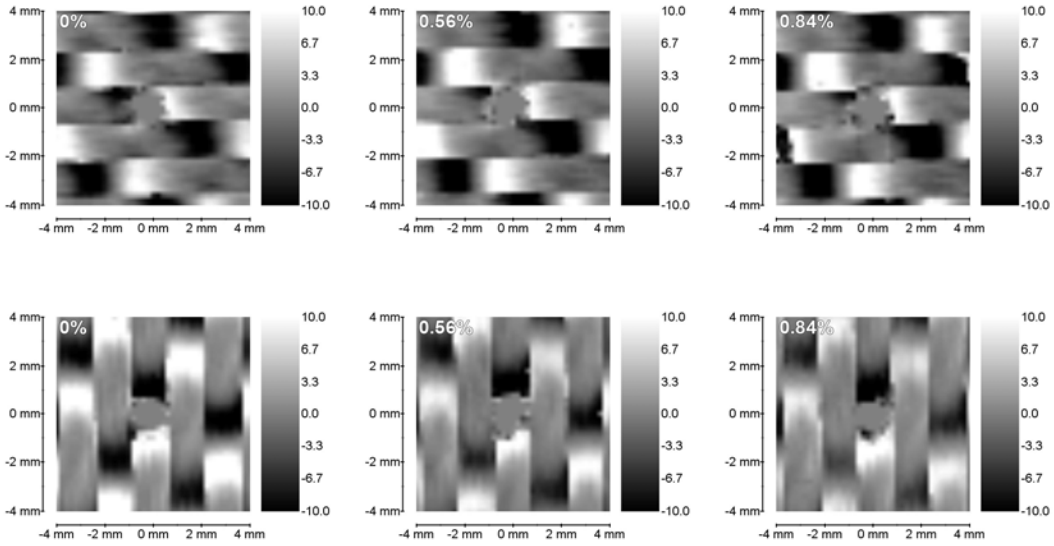

Figure 10: Average out-of-plane fibre tilt angle (in degrees) for transverse (top) and longitudinal (bottom) yarns within the satin woven composite at three different strain levels (strain axis is vertical).

This capability is demonstrated in Figure 10 for the average angle of yarn tilt out of the detector plane. This has been calculated from the ratio of meridional reflection intensities between opposing diffraction pattern hemispheres. The calculation requires a

calibration function derived empirically from a unidirectional composite having a comparable degree of intra- and inter-fibre domain orientation. It also requires layer lines with sufficiently long reciprocal scattering vectors. The example in Figure 10 is shown for the satin FRC specimen prior to deformation (i.e. unloaded). In this case, average fibre tilt is calculated for both transverse (horizontal) and longitudinal (vertical) yarns within each diffraction pattern.

The results in Figure 10 reveal that even relatively complex fabric geometries can be resolved with ease through the resin matrix. The position of the drilled hole is clearly visible at the centre of the scan region (those data points having been eliminated based upon their lower total scattering intensity). The fabric structure surrounding the hole has not been significantly damaged by the drilling process. This can be attributed to the constraining effect of the resin. The μXRD technique could provide a new experimental approach for future studies in this field. Figure 10 also shows that the transverse yarns exhibit a lower range of angular tilts compared to longitudinal yarns. This indicates that the warp yarns are transverse in this specimen (their reduced angular tilt being a consequence of their higher tension during weaving).

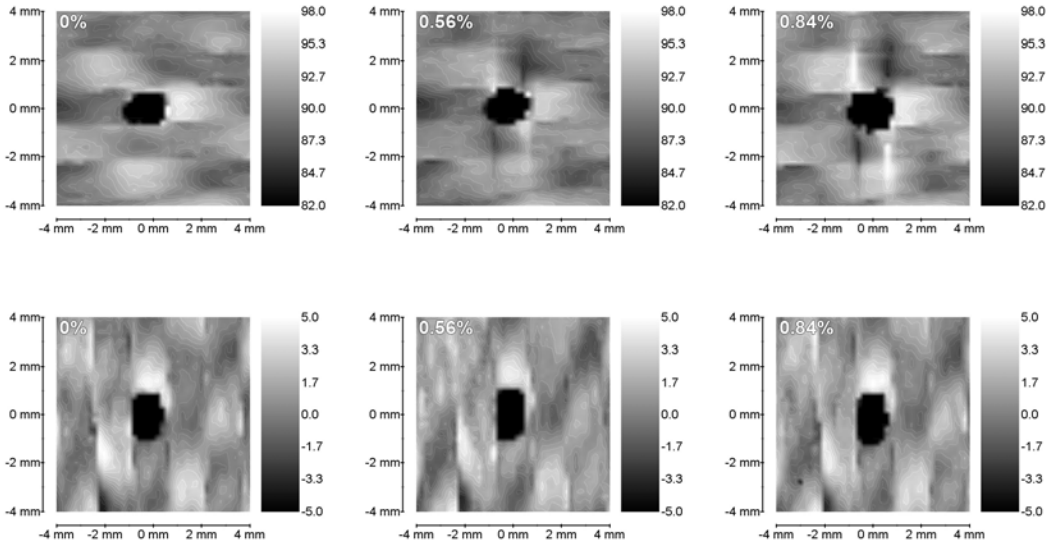

Figure 11: Average in-plane fibre orientation (in degrees) for transverse (top) and longitudinal (bottom) yarns within the woven composite at three different strain levels (strain axis is vertical).

Whilst meridional reflection intensities reveal out-of-plane yarn tilt, azimuthal reflection positions reveal yarn orientations within the detector plane. For bidirectional laminae with a sufficiently high angular difference, the in-plane orientation of the warp and weft yarns can be resolved independently. Although any reflection can be used to determine this parameter, equatorial reflections are preferred because of fibre symmetry. Figure 11 shows the average angle of in-plane yarn orientation, exclusively for transverse yarns within the satin weave composite. Prior to deformation, periodic in-plane rotations can be observed which correlate with the fabric geometry shown in Figure 10. These correspond to yarn interlace points within the fabric where yarns are displaced by the tightly-woven structure. A comparison between the undeformed and deformed plots in Figure 11 shows that deformation has no impact upon these periodic

displacements. However, new features appear during deformation, extending from the transverse edges of the drilled hole longitudinally along the stress axis. These reflect localised regions of opposing in-plane orientation (i.e. a clockwise rotation on one side of the hole and an anticlockwise rotation on the other). This demonstrates how the stress field around discontinuities such as rivet holes can influence the fabric's local geometry.

5. CONCLUSIONS

It has been demonstrated that the combination of Raman spectroscopy and X-ray diffraction give a unique insight into both the geometry of the woven structure and the micromechanics of deformation of woven composites. This allows detailed modelling of the mechanical behaviour of these important structural materials to be validated.

ACKNOWLEDGEMENTS

Dr. A. Manan is thanked for his help with the finite element analysis and Dr. Manfred Burghammer's technical support at the ID13 beamline is especially appreciated. This research was supported by the EPSRC (grant code EP/C002164/1).

References

1- Poe C.C, Dexter H.B. and Raju I.S. "A review of the NASA Textile Composites Research*,"* AIAA SDM conference 1997.

2- Drapier S. and Wisnom M.R., "F.E. investigation of the non-crimp fabrics compressive and interlaminar behaviours," *Proceedings of ICCM 12*, Paris 1999

3- N Takano, Y Uetsuji, Y Kashiwagi, M Zako, "Hierarchial modelling of textile material structures by the homogenization method," *Modelling Simul. Mater. Sci. Eng*., 1999;7: 207-231.

4- Conca C. and Vanninathan M, "Homogenization of periodic structures via bloch decomposition," *SIAM J. Appl. Math*., 2003;57:1639-1659.

5- Kim H.J. and Swan C.C., "Voxel-based meshing and unit-cell analysis of textile composites", *International Journal of Numerical Methods in Engineering*, 2003;56:977-1006.

6- Lei S.Y. and Young R.J., "Deformation of PBO/Epoxy Plain Weave Fabric Composites Followed using Raman Spectroscopy", *Composites A: Applied Science and Manufacturing*, 2001;32:499-509,.

7- Young R.J., Eichhorn S.J., Shyng Y.-T., Riekel C. and Davies R.J., "Analysis of Stress Transfer in Two-phase Polymer Systems using Synchrotron Microfocus X-ray Diffraction", *Macromolecules*, 2004;37:9503-9509.

8- Davies R.J., Eichhorn S.J., Bennett J.A., Riekel C. and Young R.J., "Analysis of the structure and deformation of a woven composite lamina using X-ray microdiffraction", *Journal of Materials Science*, in press.